Asymmetric Mushroom-Type Metamaterials

David E. Fernandes, Stanislav I. Maslovski, and Mário G. Silveirinha, *Member, IEEE*

***Abstract*—We study the scattering of electromagnetic waves by mushroom-type metamaterials such that the metallic wire array and the patch grids have different symmetry centers. Based on a quasi-static model, we develop an analytical formalism to compute the reflection and transmission characteristics of a metamaterial slab, and derive suitable boundary conditions for the patch grid interfaces. The theory is successfully compared with full-wave simulations.**

***Index Terms*—Additional boundary conditions (ABCs), high-impedance surfaces, metamaterials, wire media.**

I. Introduction

THE DESIGN of artificial ground planes and textured surfaces with tailored electromagnetic response are active fields of research, due to their important applications in wireless communications as the substrate of compact antennas [1]–[10]. Particularly, the so-called mushroom ground plane [1] continues to attract a lot of attention due to its unique characteristics, which are: 1) it provides a compact high-impedance boundary and an in-phase reflection characteristic and 2) it can suppress the propagation of guided modes. These properties are useful to enhance the radiation properties of low-profile antennas, e.g., to improve the return loss over a relatively wide bandwidth and reduce the mutual coupling in printed antenna arrays sharing the same ground plane [1]–[10]. More recently, it was shown that two-sided mushroom metamaterials (with no ground plane) enable the negative refraction of electromagnetic waves [11], [12], a partial-focusing effect [13], and superlensing [14]. Thus, mushroom-type structures are currently of great interest in microwave and millimeter-wave technologies.

Several analytical models were developed over the years that enable the accurate and fast modeling of the electromagnetic response of mushroom-type metamaterials (see, e.g., [9]–[17]). In particular, an analytical framework has been proposed ([11]–[17]) wherein the mushroom structure is regarded as a wire medium slab (modeled as a continuous medium with a spatially dispersive response [18]–[20]) capped with an impedance grid. It was shown that such a theory captures accurately the physical response of mushroom-type metamaterials in different scenarios, which include arrays of wires with and without patch grids, and wires connected to the patch grids through lumped loads.

It is known that in the conventional mushroom ground plane, the reflection characteristic for normal incidence is independent of the metallic wire array. However, for some applications it can be interesting to force an electric current to flow along the metallic wires, even when the wave that illuminates the structure impinges along the normal direction. This can be particularly useful if the metallic wires are connected to the patch grid through discrete loads. If the impedance of the load is either tunable (e.g., electronically) or if the loads have a nonlinear response, then it would be possible to control the reflection characteristics for normal incidence.

Motivated by these possibilities, this paper investigates the electromagnetic response of mushroom-type metamaterials such that the wires are asymmetrically connected to the patch grid, i.e., the connection point has an offset with respect with the geometrical center of the metallic patches. A related structure was studied in [5] using numerical techniques and with the aim of designing anisotropic ground planes with a reflection characteristic that depends on the polarization state of the incident wave. Here, we develop an effective medium approach to characterize the response of general (with and without ground plane) mushroom metamaterials such that the metallic wires are displaced from the central position of the cell. In particular, we propose suitable boundary conditions to characterize the connection of the wires to the patch grid, and prove that when the wires are displaced from the central position, the boundary conditions are such that tangential macroscopic fields become coupled with the current along the wires (or equivalently with the component of the macroscopic polarization vector normal to the interfaces).

This paper is organized as follows. In Section II, we develop the analytical model and derive the new boundary conditions. The analysis is done based on a quasi-static effective medium model for the wire medium. In Section III, we highlight the novel physical effects that result from displacing the metallic wires, and present several numerical examples—for both two-sided mushroom structures and standard mushroom ground planes—proving that the results of our theory compare well with full-wave simulations. Finally, in Section IV, the conclusions are drawn. In this work, we assume a time variation of the type $e^{-i\omega t}$, with ω being the oscillation frequency.

II. Effective Medium Model

We are interested in studying the electromagnetic response of arrays of metallic wires terminated with metallic patches at either one or at both interfaces. Moreover, we admit that the wires can be attached to the metallic patches either through a

Manuscript received July 16, 2013; revised October 29, 2013; accepted October 31, 2013. Date of publication December 03, 2013; date of current version January 06, 2014. This work was supported by the Fundação para Ciência e a Tecnologia under project PTDC/EEI-TEL/2764/2012. The work of D. E. Fernandes was supported by the Fundação para a Ciência e a Tecnologia, Programa Operacional Potencial Humano/POPH, and the cofinancing of Fundo Social Europeu under Fellowship SFRH/BD/70893/2010.

The authors are with the Departamento de Engenharia Electrotécnica, Instituto de Telecomunicações, Universidade de Coimbra Pólo II, 3030-290 Coimbra, Portugal (e-mail: dfernandes@co.it.pt; stas@co.it.pt; mario.silveirinha@co.it.pt).

Color versions of one or more of the figures in this paper are available online at http://ieeexplore.ieee.org.

Digital Object Identifier 10.1109/TMTT.2013.2291539

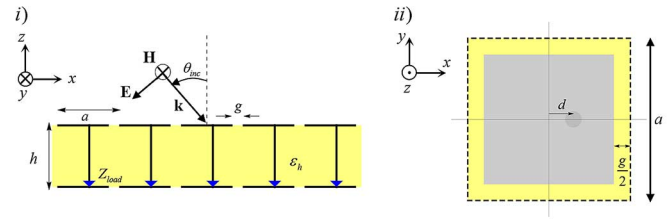

Fig. 1. Representative geometry of the problem under study (two-sided mushroom slab). (i) Side view: the wires are arranged in a periodic square lattice with period a, embedded in a dielectric host with permittivity ε_h and thickness h. The wires may be connected to the patches through lumped loads (blue arrows in online version). The separation between consecutive patches is g. The slab is illuminated by TM-polarized plane wave with angle of incidence $\theta_{\rm inc}$. (ii) Top view of one cell of the two-sided mushroom structure: the wire is displaced by d off the center of the patch in the positive x-direction.

direct (short-circuit) connection, or alternatively through a discrete lumped load. In Fig. 1, we depict a representative geometry of the system, for the case where patches are attached to the metallic wires at both interfaces and the wire and patch grids are misaligned. Related structures have been analyzed in the literature using different approaches [9]–[17], but always for the case of centered patches.

A. Bulk Wire Medium

We start by discussing the basic properties of the bulk wire medium. This metamaterial is made of long metallic wires arranged in a periodic square lattice. We suppose that the metallic wires are oriented along the z-direction and embedded in a dielectric host with permittivity ε_h. It is known from previous studies [18]–[20] that the effective dielectric function of the metamaterial is

$$\overline{\overline{\varepsilon}} = \varepsilon_h \left[\varepsilon_t(\hat{\mathbf{x}}\hat{\mathbf{x}} + \hat{\mathbf{y}}\hat{\mathbf{y}}) + \varepsilon_{zz}\hat{\mathbf{z}}\hat{\mathbf{z}}\right] \tag{1}$$

where $\varepsilon_{zz} = 1 + [(\varepsilon_h/(\varepsilon_m - \varepsilon_h)f_V) - ((\beta_h^2 - k_z^2)/k_p^2)]^{-1}$, $\beta_h = \sqrt{\varepsilon_h\mu_0}\omega$ is the wavenumber in the host medium, r_w is the wires radius, a is the lattice period, $f_V = \pi(r_w/a)^2$ is the volume fraction of the metal, ε_m is the complex permittivity of the metallic wires, and k_p is a structural parameter with the physical meaning of the plasma wave number. Within a thin wire approximation, one has $(k_p a)^2 \approx 2\pi/[0.5275 + \ln(a/2\pi r_w)]$ and the transverse permittivity satisfies $\varepsilon_t \approx 1$ [18], [19]. Without loss of generality, here we focus our attention in the microwave regime, and suppose that the metal is modeled as a perfect electric conductor (PEC) such that $\varepsilon_m = -\infty$ and $\varepsilon_{zz} = 1 - k_p^2/(\beta_h^2 - k_z^2)$. The dependence of the dielectric function on the wave vector $k_z = -id/dz$ implies a strong spatial dispersive response [18], [19].

B. Electromagnetic Field Distribution

We want to analyze the scattering of a wire medium slab with thickness h (with the wires possibly attached to metallic patches, as discussed previously) under plane wave incidence. We consider that the incoming plane wave is transverse magnetic (TM) polarized (magnetic field is along the y-direction) with an incidence angle $\theta_{\rm inc}$ so that the plane of incidence is the xoz plane. This monochromatic wave can excite plane waves in the slab with a transverse wave vector $\mathbf{k}_t = k_x\hat{\mathbf{x}} + k_y\hat{\mathbf{y}}$ such that $k_x = k_0 \sin\theta_{\rm inc}$ and $k_y = 0$ with $k_0 = \omega/c$ and c is the light speed in vacuum. The electromagnetic field inside the slab can be written in terms of the natural photonic modes of the bulk wire medium, more specifically in terms of the so-called TM, transverse electromagnetic (TEM), and transverse electric (TE) waves [18]–[20]. In our problem the TE waves are not excited, and thus the electromagnetic field in the wire medium slab is written as a superposition of four plane waves: two pairs of counter-propagating waves (propagating along $+z$- and $-z$-directions, respectively) associated with TEM and TM modes. The relevant field components in our problem are H_y, E_x, and E_z.

In the case the wire medium slab is surrounded by air (e.g., for the two-sided mushroom structured represented in Fig. 1, the magnetic field distribution in the whole space can be written as

$$H_y = e^{ik_x x}\frac{E^{\rm inc}}{\eta_0} \times \begin{cases} (e^{\gamma_0 z} - \mathrm{Re}^{-\gamma_0 z}), & z > 0 \\ A_1 e^{\gamma_{\rm TM}(z+h)} + A_2 e^{-\gamma_{\rm TM}(z+h)} + B_1 e^{\gamma_{\rm TEM}(z+h)} \\ \quad + B_2 e^{-\gamma_{\rm TEM}(z+h)}, & -h < z < 0 \\ Te^{\gamma_0(z+h)}, & z < -h \end{cases} \tag{2}$$

where R and T are the reflection and transmission coefficients, and $A_{1,2}$ and $B_{1,2}$ stand for the complex amplitudes of the TM and TEM waves, respectively, in the wire medium slab. The propagation constants of the TM and TEM modes can be determined from the dispersion equation inside the wire medium [18]–[20] $\gamma_{\rm TM} = \sqrt{k_x^2 + k_p^2 - \omega^2\varepsilon_h\mu_0}$ and $\gamma_{\rm TEM} = -i\omega\sqrt{\varepsilon_h\mu_0}$. The free-space propagation constant along the z-direction is $\gamma_0 = \sqrt{k_x^2 - \omega^2\mu_0\varepsilon_0}$, η_0 is the free-space impedance, and $E^{\rm inc}$ is the incident field complex amplitude.

Using $\mathbf{E} = (1/-i\omega)[\overline{\overline{\varepsilon}}(\omega, -i(d/dz))]^{-1}\cdot\nabla\times\mathbf{H}$, it is found that the relevant electric field components are given by

$$E_x = \frac{e^{ik_x x}}{i\omega\varepsilon_0} \cdot \frac{E^{\rm inc}}{\eta_0} \begin{cases} \gamma_0(e^{\gamma_0 z} + \mathrm{Re}^{-\gamma_0 z}), & z > 0 \\ \frac{\varepsilon_0}{\varepsilon_h}\gamma_{\rm TM}\left(A_1 e^{\gamma_{\rm TM}(z+h)} - A_2 e^{-\gamma_{\rm TM}(z+h)}\right) \\ \quad + \frac{\varepsilon_0}{\varepsilon_h}\gamma_{\rm TEM}\left(B_1 e^{\gamma_{\rm TEM}(z+h)} - B_2 e^{-\gamma_{\rm TEM}(z+h)}\right), \\ \quad -h < z < 0 \\ \gamma_0 T e^{\gamma_0(z+h)}, & z < -h \end{cases} \tag{3}$$

$$E_z = -e^{ik_x x} \cdot \frac{E^{\rm inc}}{\eta_0}\frac{k_x}{\omega\varepsilon_0} \begin{cases} e^{\gamma_0 z} - \mathrm{Re}^{-\gamma_0 z}, & z > 0 \\ \frac{\varepsilon_0}{\varepsilon_{zz}^{\rm TM}}\left(A_1 e^{\gamma_{\rm TM}(z+h)} + A_2 e^{-\gamma_{\rm TM}(z+h)}\right), \\ \quad -h < z < 0 \\ Te^{\gamma_0(z+h)}, & z < -h \end{cases} \tag{4}$$

where $\varepsilon_{zz}^{\rm TM} = \varepsilon_h k_x^2/(k_p^2 + k_x^2)$ is the permittivity along the wires for the TM polarization.

C. Overview of the Quasi-Static Wire Medium Model and of the Boundary Conditions

Solving scattering problems involving spatially dispersive media generally requires imposing additional boundary conditions (ABCs) [21]. In general, ABCs are needed for both connected and non-connected wire media [17]–[24]. In previous works [17]–[24], it was found that the ABCs are intrinsically related to the behavior of microscopic electric charge density and microscopic electric current at the wire ends.

A convenient framework to model wire media was developed in [20] and [24], and is based on a quasi-static approximation. Within this approach, the electrodynamics of the effective medium is described not only in terms of the macroscopic fields $(\mathbf{E}, \mathbf{H})$, but also in terms of two scalar variables (I, φ_w), with the physical meaning of current along the wires and quasi-static potential, respectively. In general, the quasi-static potential φ_w can be regarded as the average potential drop from a given wire to the boundary of the respective unit cell [20], [25]

$$\varphi_w \approx \frac{1}{2\pi}\int_0^{2\pi}\int_{r_w}^{\frac{a}{2}} \mathbf{e}\cdot\hat{\boldsymbol{\rho}}\; d\;\rho d\theta \tag{5}$$

where (ρ, θ, z) represents a system of cylindrical coordinates centered at the pertinent metallic wire with radius r_w, and $\mathbf{e}$ denotes the microscopic electric field (before the spatial averaging is done).

Both the current and the quasi-static potential are interpolated in such a manner that they can be regarded as continuous functions of space. It was proven in [20] that the dynamics of the state variables $(\mathbf{E}, \mathbf{H}, I, \varphi_w)$ is described by a system of coupled Maxwell and "transmission line"-type equations. In the absence of field sources and for PEC wires oriented along the z-direction, one has

$$\nabla\times\mathbf{E} = +i\omega\mu_0\mathbf{H} \tag{6a}$$

$$\nabla\times\mathbf{H} = -i\omega\varepsilon_h\mathbf{E} + \frac{I}{a^2}\hat{\mathbf{z}} \tag{6b}$$

$$\frac{\partial I}{\partial z} = i\omega C_w\varphi_w \tag{6c}$$

$$\frac{\partial \varphi_w}{\partial z} = i\omega L_w I + E_z. \tag{6d}$$

where L_w is a per unit of length (p.u.l.) wire inductance and C_w is a p.u.l. wire capacitance given by [20]

$$L_w = \frac{\mu_0}{2\pi}\log\left(\frac{a^2}{4r_w(a-r_w)}\right)$$

$$C_w = \varepsilon_h\left[\frac{1}{2\pi}\log\left(\frac{a^2}{4r_w(a-r_w)}\right)\right]^{-1}. \tag{7}$$

The spatially dispersive dielectric function (1) can be recovered by eliminating the additional variables (I, φ_w) in favor of $(\mathbf{E}, \mathbf{H})$ [20], [24].

The interesting thing about this quasi-static approach is that it provides a natural framework to formulate boundary conditions at the wire medium interfaces. Indeed, since the electrodynamics of the wire medium is described in terms of a eight component state variable $(\mathbf{E}, \mathbf{H}, I, \varphi_w)$, typically one must provide boundary conditions not only for $(\mathbf{E}, \mathbf{H})$, as in standard dielectric media, but also boundary conditions for (I, φ_w) [24]. The latter correspond to the previously mentioned ABCs.

Based on these ideas, it was demonstrated in [24] that for a boundary corresponding to wires connected to patches at the central point (with no lumped loads), the quasi-static potential φ_w satisfies the following boundary condition at the interface $z = z_0$:

$$\varphi_w = \frac{Q}{C_{\text{patch}}} = \frac{I}{-i\omega C_{\text{patch}}}\hat{\mathbf{n}}\cdot\hat{\mathbf{z}}, \qquad \text{at } z = z_0 \tag{8}$$

where Q is the charge stored at the patch, and $\hat{\mathbf{n}}$ is the outward unit vector directed toward the exterior of the wire medium, e.g., at the upper (lower) interface in Fig. 1 $\hat{\mathbf{n}} = \hat{\mathbf{z}}$ $(\hat{\mathbf{n}} = -\hat{\mathbf{z}})$. At an interface with air, the patch capacitance is given by [20]

$$C_{\text{patch}} = (\varepsilon_h + \varepsilon_0)\pi(a-g)\frac{1}{\log\left(\sec\left(\frac{\pi g}{2a}\right)\right)}. \tag{9}$$

where g represents the spacing between two adjacent patches (Fig. 1). Using (6c), it is possible to rewrite (8) in terms of the current I as follows:

$$\frac{\partial I}{\partial z} + \frac{C_w}{C_{\text{patch}}}(\hat{\mathbf{n}}\cdot\hat{\mathbf{z}})I = 0, \text{ at } z = z_0. \tag{10}$$

On the other hand, in the same scenario, the macroscopic electromagnetic fields satisfy the boundary conditions

$$\lfloor E_x\rfloor_{z=z_0} = 0 \tag{11}$$

$$\lfloor H_y\rfloor_{z=z_0} = -Y_g E_x|_{z=z_0} \tag{12}$$

where $Y_g = -i(\varepsilon_h + \varepsilon_0)(\omega a/\pi)\log[\csc(\pi g/2a)]$ is the effective patch grid admittance [26], and the operator $\lfloor\;\rfloor_{z=z_0}$ represents the difference between the operand calculated at the two sides of an interface so that $\lfloor F\rfloor_{z=z_0} = F|_{z=z_0^+} - F|_{z=z_0^-}$. From a macroscopic point of view, the grid may be regarded as an electric current sheet. As a consequence, the tangential components of the electric field are continuous [see (11)] and the macroscopic surface current is related to the macroscopic tangential electric field through an impedance boundary condition $\hat{\mathbf{z}}\times\lfloor\mathbf{H}\rfloor_{z=z_0} = Y_g\mathbf{E}_{\tan}|_{z=z_0}$ [see (12)].

Equations (10)–(12) are the boundary conditions at an interface of air and a wire medium attached to a patch grid. The ABC (10) can be rewritten in terms of the macroscopic electromagnetic fields using the formula [24]

$$J_z = \frac{I_z}{a^2} = +i\omega\varepsilon_h E_z + \hat{\mathbf{z}}\cdot(i\mathbf{k}_t\times\mathbf{H}_t) \tag{13}$$

where $\mathbf{k}_t, \mathbf{H}_t$ stand for the transverse (to z) components of the wave vector and magnetic field, respectively, which are given by $\mathbf{k}_t = k_x\hat{\mathbf{x}}$, $\mathbf{H}_t = \mathbf{H} = H_y\hat{\mathbf{y}}$ in our problem. Hence, one can impose all the boundary conditions directly on the macroscopic electromagnetic fields [see (2)–(4)], and in this manner solve the scattering problem [24].

D. Boundary Conditions for Off-Centered Patches

Now we come to the main novelty of this work, which is the generalization (10)–(12) to the case wherein the metallic wires

are displaced with respect to the center of the patches. To do this, we start by noting that the microscopic electric field $\mathbf{e}$ in the vicinity of a given patch has two contributions. The first contribution, which we denote by $\mathbf{e}_{a-\mathrm{sym}}$, is a response to an external applied field (and to the charges induced on other patches by this external field). This external field induces a distributed charge density $\sigma_{a-\mathrm{sym}}$ over the patch surface. The second contribution, denoted by $\mathbf{e}_{\mathrm{sym}}$, is the field created by the electric charge density σ_{sym} associated with the charges stored in the metallic patches as a result of the patches being connected to metallic wires. In other words, σ_{sym} describes the charges transported to the patches through the metallic wires. It should be clear that the total charge stored in a metallic patch is $Q = Q_{\mathrm{sym}} + Q_{a-\mathrm{sym}} = Q_{\mathrm{sym}}$ because $Q_{a-\mathrm{sym}}$ vanishes ($Q_i = \int_{\mathrm{patch}} \sigma_i ds$).

From (5), the quasi-static potential in the vicinity of a metallic patch can be decomposed as

$$\varphi_w = \varphi_{w,\mathrm{sym}} + \varphi_{w,a-\mathrm{sym}} \tag{14}$$

where $\varphi_{w,i} = (1/2\pi)\int_0^{2\pi}\int_{r_w}^{a/2} \mathbf{e}_i \cdot \hat{\boldsymbol{\rho}} d\rho d\theta$ with $i = a-\mathrm{sym}, \mathrm{sym}$. Hence, based on symmetry arguments, when the patch is centered at the origin (being the origin taken as the position of the pertinent metallic wire), it follows that $\varphi_{w,a-\mathrm{sym}} \approx 0$. Thus, in the usual configuration wherein the patches are centered with respect to the metallic wires, we have $\varphi_w = \varphi_{w,\mathrm{sym}}$, i.e., the quasi-static potential is created by the charges stored in the patches [20]. From (8), we can infer that

$$\varphi_{w,\mathrm{sym}} = \frac{Q_{\mathrm{sym}}}{C_{\mathrm{patch}}} = \frac{I}{-i\omega C_{\mathrm{patch}}} \hat{\mathbf{n}} \cdot \hat{\mathbf{z}}. \tag{15}$$

It will be assumed that to a first approximation this formula holds with no corrections for off-centered patches.

However, for off-centered patches, the symmetry of the fields with respect to the unit-cell center is broken, and in general, $\varphi_{w,a-\mathrm{sym}} \neq 0$. Let us estimate $\varphi_{w,a-\mathrm{sym}}$ in case $d \approx (a-g)/2$, i.e., when the metallic wire is attached to a point close to the border of the metallic patch. In such a case, the integral $\int_{r_w}^{a/2} \mathbf{e}_{a-\mathrm{sym}} \cdot \hat{\boldsymbol{\rho}} d\rho$ is negligible for $\pi/2 < |\theta| < \pi$ because the integration path is over a single metallic patch (see the path C_1 in Fig. 2). On the other hand, for $|\theta| < \pi/2$ (see path C_2 in Fig. 2), the integral $\int_{r_w}^{a/2} \mathbf{e}_{a-\mathrm{sym}} \cdot \hat{\boldsymbol{\rho}} d\rho$ is nothing more than the potential difference between two adjacent patches (along the x-direction). Within a quasi-static approximation, this potential difference is constant and equal to $E_x a$. From these results, it follows that

$$\varphi_{w,a-\mathrm{sym}} = \int_0^{2\pi}\int_{r_w}^{\frac{a}{2}} \frac{\mathbf{e}_{a-\mathrm{sym}}}{2\pi} \cdot \hat{\boldsymbol{\rho}} d\rho d\theta \approx \int_{-\pi/2}^{\frac{\pi}{2}} \frac{E_x a}{2\pi} d\theta = \frac{1}{2} E_x a, \quad \text{for } d \approx \frac{(a-g)}{2}. \tag{16}$$

As discussed previously, $\varphi_{w,a-\mathrm{sym}}|_{d=0} = 0$. We estimate $\varphi_{w,a-\mathrm{sym}}$ using simply a linear interpolation of the offset d, and thus we will use

$$\varphi_{w,a-\mathrm{sym}} \approx E_x a f_\alpha, \qquad \text{with } f_\alpha = \frac{d}{a-g}. \tag{17}$$

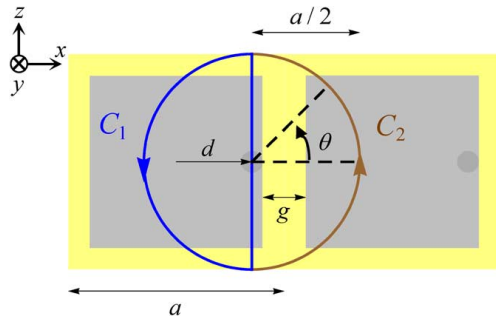

Fig. 2. Sketch of the integration paths used to calculate the potential $\varphi_{w,a-\mathrm{sym}}$ when the wire is displaced from the center of the unit cell and located near a point on the border of the patch. The path is divided into two distinct sub-paths corresponding to variations on the azimuthal angle such that $\pi/2 < |\theta| < \pi$ corresponds to path C_1 and $|\theta| < \pi/2$ to path C_2.

Note that the parameter f_α varies in the range $-(1/2) < f_\alpha < (1/2)$, and is positive (negative) for positive (negative) wire displacements d.

From (14), (15), and (17), we see that the quasi-static potential at the connection between a metallic wire and a metallic patch satisfies

$$\varphi_w = \frac{I}{-i\omega C_{\mathrm{patch}}} \hat{\mathbf{n}} \cdot \hat{\mathbf{z}} + E_x a f_\alpha, \qquad \text{at } z = z_0. \tag{18}$$

This result generalizes (8), and is the sought ABC for an interface ($z = z_0$) wherein the wires are connected to off-centered patches. When the wires are connected to the metallic patches through a lumped load with impedance Z_{Load}, (18) needs to be modified as follows [24]:

$$\varphi_w = \left(\frac{1}{-i\omega C_{\mathrm{patch}}} + Z_{\mathrm{load}}\right) I(\hat{\mathbf{n}} \cdot \hat{\mathbf{z}}) + E_x a f_\alpha, \qquad \text{at } z = z_0. \tag{19}$$

Similar to Section II-C, with the help of (6c), it is possible to rewrite the above condition in terms of the current density $J_z = I/a^2$, as follows:

$$\frac{\partial J_z}{\partial z} + \left(\frac{C_w}{C_{\mathrm{patch}}} - i\omega C_w Z_{\mathrm{load}}\right) J_z(\hat{\mathbf{n}} \cdot \hat{\mathbf{z}}) - i\omega C_w f_\alpha \frac{1}{a} E_x = 0, \qquad \text{at } z = z_0. \tag{20}$$

Using (13), one can impose this ABC directly on the macroscopic electromagnetic fields.

It is interesting to note that the boundary condition (19) implies that the wire termination with an off-centered patch can be equivalently represented by a termination with a centered patch of the same dimensions and a controlled voltage source $V^{as} = E_x a f_\alpha$ (see Fig. 3). In this circuit, the voltage source V^{as} accounts for the current induced in the wires by the tangential electric field applied to the off-centered patch grid.

Next, we discuss how the two boundary conditions (11) and (12) are modified for off-centered patches. Clearly, independent of the displacement d, the patch grid can always be regarded from a macroscopic point of view as an electric current sheet, and this implies that the boundary condition for the electric field [see (11)] remains the same. However, because the general Onsager–Casimir symmetry principle [27], [28] (i.e., reciprocity principle), the equivalent circuit of Fig. 3 suggests that (12) needs be modified to take into account the reverse effect

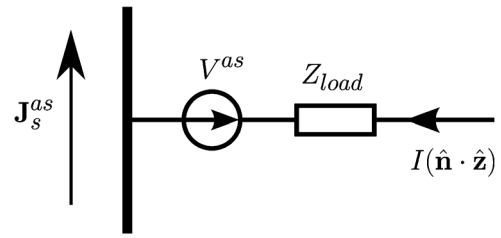

Fig. 3. Termination of a wire with an off-centered patch can be represented by a centered patch of the same dimensions and a pair of controlled voltage and current sources.

of polarizing the off-centered patch grid by the wire current. To clarify this, we start by noting that for centered patches, the effective density of surface current $\mathbf{J}_s = \hat{\mathbf{z}} \times \lfloor \mathbf{H} \rfloor_{z=z_0}$ induced on the grid depends only on the macroscopic electric field $\mathbf{E}$. Indeed the microscopic surface current associated with the charge $Q_{\rm sym}$ has a radial-type profile for centered patches, and hence, cannot contribute to the effective macroscopic surface current $\mathbf{J}_s$. However, for off-centered patches, the symmetry is broken and thus $\mathbf{J}_s$ may depend on both $\mathbf{E}$ and $Q_{\rm sym}$, or equivalently (because $Q_{\rm sym}$ is the charge transported by the current I) may depend on both $\mathbf{E}$ and I. This can be taken into account by writing the total surface current in the patch grid plane as $\mathbf{J}_s = Y_g E_x \hat{\mathbf{x}} + \mathbf{J}_s^{as}(I)$. In terms of the equivalent representation shown in Fig. 3 this corresponds to introducing another controlled source in the model: the sheet of surface current $\mathbf{J}_s^{as} = \mathbf{J}_s^{as}(I)$. Assuming for simplicity that the linear dependence of $\mathbf{J}_s^{as}$ on I is to a first approximation local (i.e., it does not depend on spatial derivatives of the current), we can write $\mathbf{J}_s^{as} = -BI\hat{\mathbf{x}}$, which leads to the following boundary condition that generalizes (12):

$$\lfloor H_y \rfloor_{z=z_0} = -Y_g E_x|_{z=z_0} + BI. \tag{21}$$

In the above, B is a constant yet to be determined. To calculate B, we appeal to reciprocity arguments.

In the Appendix, we derive the Lorentz lemma and the reciprocity theorem for the general case of uniaxial wire media with embedded sources. One may directly apply this theorem to the equivalent circuit of Fig. 3 if the controlled sources V^{as} and $\mathbf{J}_s^{as}$ are understood as external sources embedded into a regular wire medium. The controlled sources model the electromagnetic response of the metallic patches. By considering two scenarios of excitation of the structure shown in Fig. 3 with either $V_1^{as} = 0$, $\mathbf{J}_{s,1}^{as} \neq 0$ or $V_2^{as} \neq 0$, $\mathbf{J}_{s,2}^{as} = 0$, we obtain from the reciprocity theorem [(A5) with $V^{\rm ext} = -(\hat{\mathbf{n}}\cdot\hat{\mathbf{z}})V^{as}\delta(z-z_0)$ and $\mathbf{J}^{\rm ext} = \mathbf{J}_s^{as}\delta(z-z_0)$] that

$$E_{x,2}\hat{\mathbf{x}}\cdot\mathbf{J}_{s,1}^{as} = -\frac{V_2^{as} I_1(\hat{\mathbf{n}}\cdot\hat{\mathbf{z}})}{a^2}. \tag{22}$$

From here, $-E_{x,2}BI_1 = (-E_{x,2}af_\alpha I_1(\hat{\mathbf{n}}\cdot\hat{\mathbf{z}})/a^2)$ or $B = (f_\alpha/a)(\hat{\mathbf{n}}\cdot\hat{\mathbf{z}})$.

The same result can be obtained in a slightly more cumbersome manner, but without employing equivalent sources. Indeed, from the results of the Appendix, it follows that the volume integral on the right-hand side of (A4) vanishes in a reciprocal background. Therefore, when applied to a generic interface of our geometry (let us say $z = z_0$), the reciprocity theorem [(A4) applied to a small pill box enclosing the interface] requires that $\hat{\mathbf{n}}\cdot[\mathbf{E}_1\times\mathbf{H}_2 - \mathbf{E}_2\times\mathbf{H}_1 + ((\varphi_{w,1}I_2 - \varphi_{w,2}I_1)/a^2)\hat{\mathbf{z}}]$ is continuous across the interface for two generic field distributions labeled with the indices 1 and 2. Considering an interface with air, this implies that

$$E_{1,x}^{WM}H_{2,y}^{WM} - E_{2,x}^{WM}H_{1,y}^{WM}\big|_{z=z_0} + \left.\frac{\varphi_{w,1}I_2 - \varphi_{w,2}I_1}{a^2}\right|_{z=z_0} = E_{1,x}^{\rm air}H_{2,y}^{\rm air} - E_{2,x}^{\rm air}H_{1,y}^{\rm air}\big|_{z=z_0} \tag{23}$$

where the subscripts WM and *air* indicate at which side of the interface the fields are evaluated (the current and additional potential vanish at the air side). From (11), the electric field is continuous (hence, it is simply denoted by E_x), and thus we can rewrite the previous equation as

$$-\hat{\mathbf{n}}\cdot\hat{\mathbf{z}}\left(E_{1,x}\lfloor H_{2,y}\rfloor_{z=z_0} - E_{2,x}\lfloor H_{1,y}\rfloor_{z=z_0}\right) + \left.\frac{\varphi_{w,1}I_2 - \varphi_{w,2}I_1}{a^2}\right|_{z=z_0} = 0. \tag{24}$$

Using now (19) and (21), it seen that

$$\left(-\hat{\mathbf{n}}\cdot\hat{\mathbf{z}}B + \frac{f_\alpha}{a}\right)(E_{1,x}I_2 - E_{2,x}I_1) = 0. \tag{25}$$

In order that this condition can hold for arbitrary field distributions, it is required that $B = (f_\alpha/a)\hat{\mathbf{n}}\cdot\hat{\mathbf{z}}$, i.e., we arrive at the same result as with the use of the equivalent model. Using the expression for the Poynting vector in wire media derived in [29], it is straightforward to prove that, in the lossless case, this result also ensures the continuity of the power flow across an interface with the wire medium.

E. Summary

The findings of Section II-D are summarized in the following equations that give the boundary conditions at an interface ($z = z_0$) between air and a wire medium slab attached to a misaligned patch grid:

$$\lfloor E_x \rfloor_{z=z_0} = 0 \tag{26a}$$

$$\lfloor H_y \rfloor_{z=z_0} = -Y_g E_x|_{z=z_0} + \frac{f_\alpha}{a}\hat{\mathbf{n}}\cdot\hat{\mathbf{z}}I \tag{26b}$$

$$\frac{\partial J_z}{\partial z} + \left(\frac{C_w}{C_{\rm patch}} - i\omega C_w Z_{\rm load}\right)J_z(\hat{\mathbf{n}}\cdot\hat{\mathbf{z}}) - i\omega C_w f_\alpha \frac{1}{a}E_x = 0 \tag{26c}$$

By imposing these boundary conditions on the electromagnetic fields [see (2)–(4)] with the help of (13), one can obtain a linear system of equations and compute the scattering parameters and the field distribution everywhere in space. It is interesting to note that for misaligned patches, the boundary conditions for (26b) and (26c) involve both (I, φ_w) and $(\mathbf{E}, \mathbf{H})$, that is the "electromagnetic part" of the system that is coupled to the "transmission

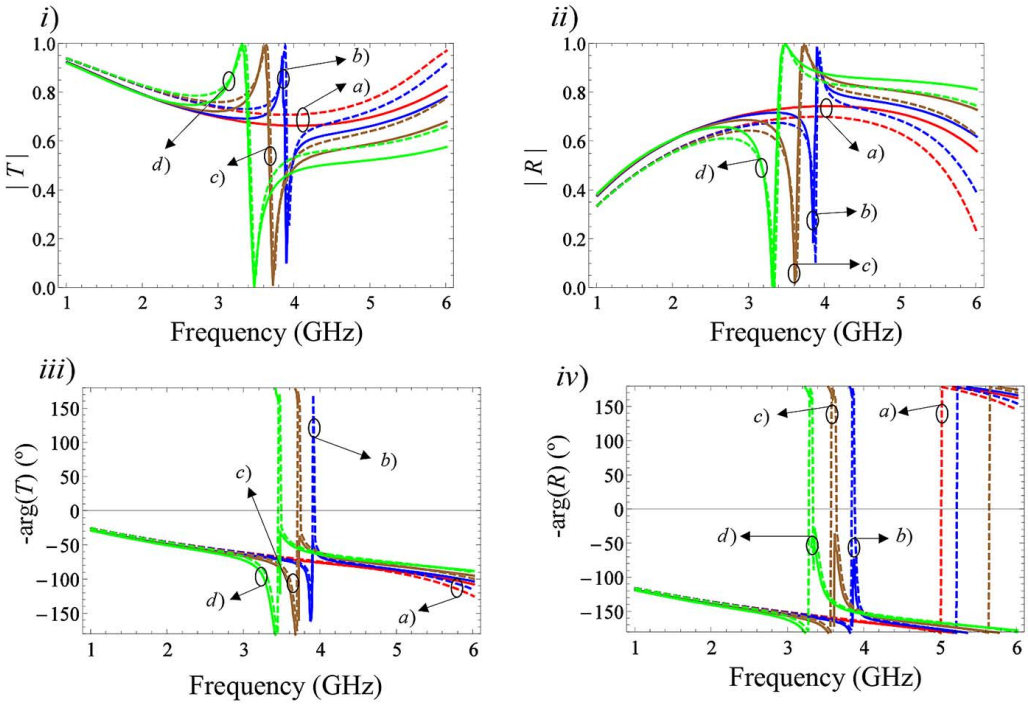

Fig. 4. Representation of the: (i) magnitude and (iii) phase of the transmission coefficient and (ii) the magnitude and (iv) phase of the reflection coefficient for a two-sided mushroom structure illuminated by a TM polarized plane wave with $\theta_{\rm inc} = 0^\circ$ for different values of the wire displacement: a) $d = 0$, b) $d = a/9$, c) $d = 2a/9$, and d) $d = a/3$. Solid lines: homogenization model; Dashed lines: full-wave simulations.

line part" not only through the dynamic equations [see (6)], but also through the boundary conditions.

The boundary conditions can be readily generalized to other scenarios. For instance, when the wire medium is attached to a PEC ground plane (i.e., when the gap g between the patches is closed) (26) should be replaced by

$$E_x\big|_{z=z_0} = 0 \tag{27a}$$

$$\frac{\partial J_z}{\partial z} + (-i\omega C_w Z_{\rm load}) J_z(\hat{\mathbf{n}} \cdot \hat{\mathbf{z}}) = 0. \tag{27b}$$

III. Examples and Discussion

Next, we consider several numerical examples that illustrate the application of our theory to metamaterial slabs with different geometries.

A. Two-Sided Mushroom Slab With Displaced Wires

To begin with, we consider a two-sided mushroom slab (Fig. 1) with the following structural parameters: slab thickness $h = 2a/9$; patch separation $g = a/9$ and lattice period $a = 18$ mm. The wires are PEC, have radius $r_w = a/72$, and stand in air. We assume that the wires are connected to the patches through a perfect short-circuit ($Z_{\rm load} = 0$), and suppose that the incidence angle is $\theta_{\rm inc} = 0^\circ$ (normal incidence).

In Fig. 4, we compare the results obtained with our homogenization model and the commercial full-wave electromagnetic simulator Microwave Studio [30] for several values of the displacement of the wires, d. One can see that there is a good agreement between effective medium approach and the full-wave simulations, supporting the validity of our theory. This indicates that the boundary conditions (26) model accurately the dynamics of the state variables near the interfaces. The small difference between the results is of the same order as that obtained for the case of centered patches [17]–[21] and is a consequence of the approximations implicit in the analytical model.

Moreover, the results show that the relative position of the wires in the cell has a major influence in the behavior of the reflection and transmission properties. For normal incidence, it is seen that displacing the wires leads to the emergence of a new resonance. This happens because (I, φ_w) and $(\mathbf{E}, \mathbf{H})$ become coupled through the boundary conditions. The resonance frequency shifts to lower values as we increase the offset of the wires with respect to the central position in the cell. This is expected because such a change effectively results in a physically larger oscillation path for the electrons on the patches (the oscillation path contains the metallic wire), and this leads to a reduction of the resonance frequency. The new resonance is seen only when the symmetry of the structure is broken, and for small values of d it is associated with an odd-type mode that cannot be excited with a slow-varying incoming plane wave. Similar odd-type resonances have been reported elsewhere [31], [32].

Previous studies [17]–[21] have shown that inserting lumped loads at the wire-to-patch connection may change the behavior of the scattering parameters and alter dramatically the position of the transmission resonances. To illustrate this, next we consider that lumped inductive and/or capacitive loads are inserted in the bottom grid, i.e., at $z = -h$. By considering an effective load impedance given by [24]

$$Z_{\rm load,eff} = -i\omega L_{\rm par} + \frac{1}{-i\omega C_{\rm par} + \left(\dfrac{1}{Z_{\rm load}}\right)} \tag{28}$$

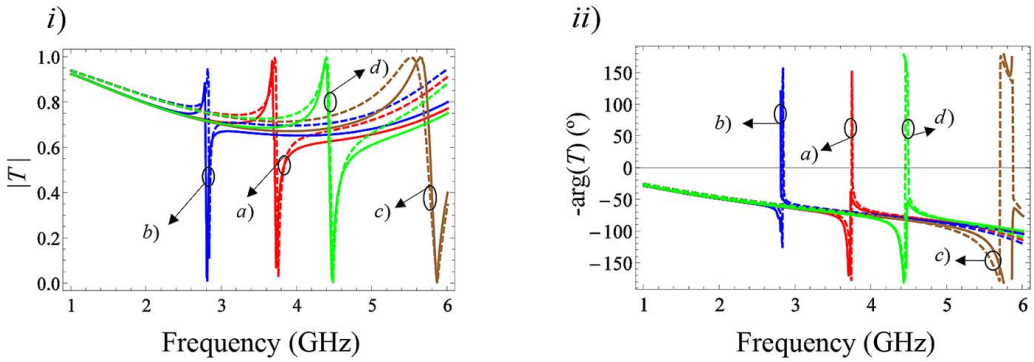

Fig. 5. Representation of: (i) magnitude and (ii) phase of the transmission coefficient for the two-sided mushroom structure with $d = a/9$ under the excitation of a TM polarized plane wave with the angle of incidence $\theta_{\rm inc} = 7.5°$ when the wires are connected to the bottom patch grid through inductive loads: a) $L = 0.2$ nH and b) $L = 2$ nH and capacitive loads c) $C = 0.4$ pF and d) $C = 2$ pF. Solid lines: homogenization model; dashed lines: full-wave simulations.

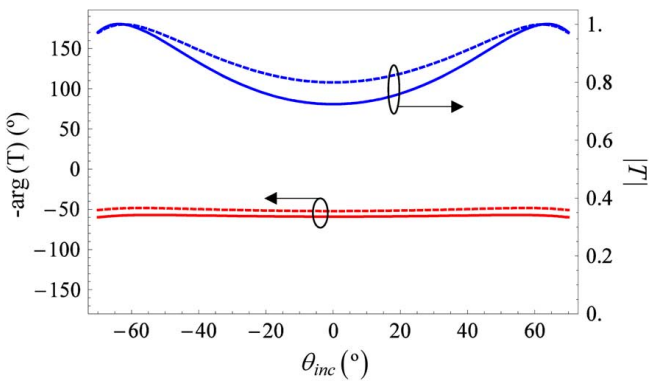

Fig. 6. Magnitude and phase of the transmission coefficient for the two-sided mushroom structure with $d = -a/9$ when the wires are connected to the bottom patch grid through an ideal short circuit for a fixed frequency $f = 2.7$ GHz as a function of the incidence angle of a TM polarized plane-wave. Solid lines: homogenization model; dashed lines: full-wave simulations.

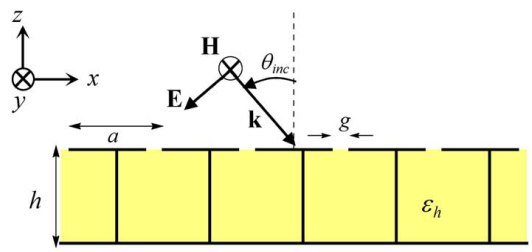

Fig. 7. Similar to panel: i) of Fig. 1, but for wires connected to a ground plane at the bottom interface.

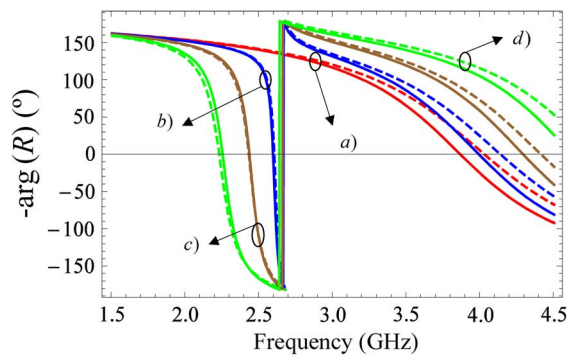

Fig. 8. Phase of the reflection coefficient for the mushroom structure terminated with a ground plane illuminated by TM-polarized wave propagating along the normal direction for different values of the offset of the wires: a) $d = 0$, b) $d = a/9$, c) $d = 2a/9$, and d) $d = a/3$. Solid lines: homogenization model; dashed lines: full-wave simulations.

it is possible to take into account the effects of parasitic capacitances and inductances ($C_{\rm par}$ and $L_{\rm par}$), which depend on the specific geometric details of the connection point.

Fig. 5 depicts the transmission characteristic of a two-sided mushroom slab where the wires are displaced by $d = a/9$ along the x-direction from the center of the patch, under the excitation of a TM wave with angle of incidence $\theta_{\rm inc} = 7.5°$ for different values of load impedance. In the full-wave simulations, we considered that the load is placed across a gap of 0.04 mm. The values of the parasitic inductance and capacitance may be estimated by curve matching between the homogenization and the full-wave simulation results. The parasitic effects introduced by the gap are well modeled by a parasitic inductance $L_{\rm par} = 0.02$ nH and parasitic capacitance $C_{\rm par} = 0.12$ pF.

As seen in Fig. 5, an increase in the inductance of the lumped load causes the transmission resonance to shift to lower frequencies, and the opposite behavior is observed when capacitive loads are considered. Thus, the lumped loads provide additional degrees of freedom to control the response of the metamaterial surface. Moreover, the proper tuning of the value of the load may allow for a switch-type behavior because the magnitude of the transmission and reflection parameters can vary very fast in a range of a few hundred megahertz.

In the previous examples, the angle of incidence was close to the normal direction. In order to validate the model for oblique incidence, we show in Fig. 6 the transmission characteristic of a two-sided mushroom slab for wide incident angles, when the wires are displaced by $d = -a/9$ along the x-direction at the fixed frequency $f = 2.7$ GHz. The wires are connected to the metallic patches through an ideal short circuit. Very interestingly, in this example, the transmission characteristic is an even function of $\theta_{\rm inc}$, or equivalently, it is seen that despite the lack of symmetry of the structure, the transmission characteristic remains invariant if $d = -a/9$ is replaced by $d = a/9$. This can be understood by noting that, in general, for a fixed $\theta_{\rm inc}$ and a fixed polarization, our system is equivalent to a four-port microwave network. The four propagation channels correspond to

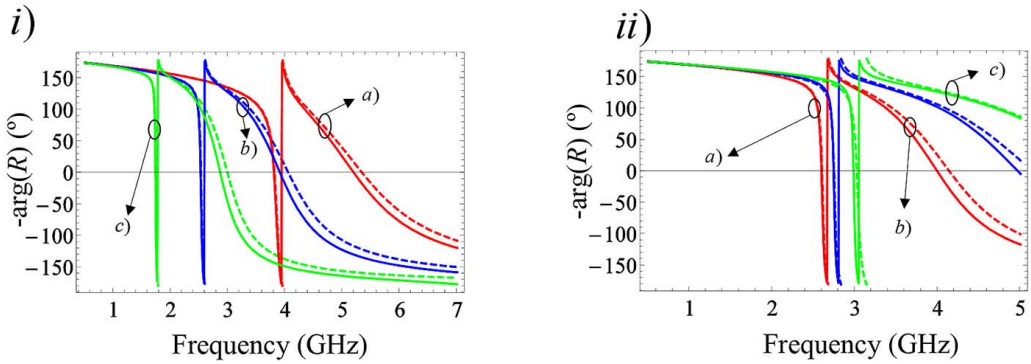

Fig. 9. Phase of the reflection coefficient for a mushroom ground plane illuminated by a TM polarized wave propagating along the normal direction for: (i) different values of the permittivity of the substrate a) $\varepsilon_h = 1$, b) $\varepsilon_h = 2.33$, and c) $\varepsilon_h = 5$ and (ii) different values of the separation between patches a) $g = a/9$, b) $g = 2a/9$, and c) $g = a/3$. Solid lines: homogenization model; dashed lines: full-wave simulations.

the directions $\pm\theta_{\rm inc}$ in the upper and lower subspaces. Hence, because of the reciprocity theorem, it follows that the reflection coefficient is an even function of $\theta_{\rm inc}$. On the other hand, the conservation of energy and the even parity of the reflection coefficient ensure that if the system is lossless (as in this example), the magnitude of the transmission coefficient is also an even function of $\theta_{\rm inc}$. This justifies the results of Fig. 6.

B. Mushroom Ground Plane With Displaced Wires

Next, we apply the proposed homogenization model to a conventional mushroom-type ground plane such that the wires are connected to a ground plane at the bottom interface, and to the patch grid at the top interface (Fig. 7). As before, the wire-medium slab has thickness h, the separation between consecutive patches is g, and the wires are displaced from the central position of the cell by a distance d as in panel (ii) of Fig. 1.

In the analytical model, the boundary conditions at the bottom interface are different from the ones at the top interface (see the discussion in Section II-E). In the first example, we calculate the scattering parameters for a mushroom slab with thickness $h = 2a/9$ with $g = a/9$ and for a lattice period $a = 18$ mm. The PEC wires are embedded in a host material with relative permittivity $\varepsilon_h = 2.2$ and have radius $r_w = a/72$. In Fig. 8, we compare the results obtained with our homogenization model and those computed using the full-wave simulator [30] for several values of the offset of the wires, d, supposing that the structured slab is illuminated by a TM-polarized plane wave propagating along the normal direction.

Again, a quite good agreement is observed, further validating our theory. The results are also in excellent agreement with what was reported in [5], where the same structure was analyzed, and it was shown that by offsetting the wires the reflection properties of the system can be tuned.

We also investigated the validity of the model when the structural parameters are varied. Fixing the value of the displacement the wires equal to $d = a/9$, we calculated the phase of the reflection coefficient for different values for the substrate permittivity and patch size (Fig. 9), keeping the remaining parameters as in the previous example.

It is seen in Fig. 9 that the analytical model works quite well in the considered scenarios. As expected, as the host permittivity increases, the resonant behavior (corresponding to the in-phase reflection condition) shifts to lower frequencies. Moreover, when the spacing between patches is increased, the structure resembles more and more a Fakir's bed of nails [33] (wires are terminated with an open circuit), and hence, the resonant frequency increases. Although it is noticeable that our homogenization model works better for large patches, the results are still quite acceptable for relatively small patches.

IV. Conclusion

We have developed an effective medium approach to solve scattering problems involving asymmetric mushroom-type metamaterials. It was shown that when the symmetry centers of the patch grid and wire array are misaligned, the response of the structure is drastically changed and new resonances can emerge, even for normal incidence. This occurs because in case of misaligned arrays, the electric polarizability xz component, $\alpha_{e,xz}$, of the basic inclusion in the unit cell does not vanish. This effect and the possibility to load the wires with lumped nonlinear loads may provide the opportunity to design novel tunable nonlinear electromagnetic-bandgap metamaterials in the microwave regime.

Appendix
Lorentz Lemma and the Reciprocity Theorem for the Uniaxial Wire Medium

Let us consider an unbounded uniaxial wire medium oriented along the z-coordinate, with position-dependent constitutive parameters $\varepsilon_h = \varepsilon_h(z)$, $L_w = L_w(z)$, and $C_w = C_w(z)$. When there are no external sources embedded into the wire medium, the electrodynamics are governed by the system of equations (6a)–(6d). A more general form of the field equations with external sources was derived in [29]

$$\nabla \times \mathbf{E} = +i\omega\mu_0\mathbf{H} \tag{A1a}$$

$$\nabla \times \mathbf{H} = -i\omega\varepsilon_h\mathbf{E} + \frac{I}{a^2}\hat{\mathbf{z}} + \mathbf{J}^{\rm ext} \tag{A1b}$$

$$\frac{\partial I}{\partial z} = i\omega C_w\varphi_w \tag{A1c}$$

$$\frac{\partial \varphi_w}{\partial z} = i\omega L_w I + E_z + V^{\rm ext}. \tag{A1d}$$

Here, the source term $\mathbf{J}^{\rm ext}$ can be regarded as the current density distributed in the space surrounding the wires, while

$V^{\rm ext}$ is the linear density of localized voltage sources embedded into the wires (see [29] for more details). Note that the above formulation with position-dependent constitutive parameters is applicable without modifications to the cases of stratified wire media, including the case wherein the wires occupy a half space (in the latter case, the regions free of wires can be modeled as the regions filled with wires of zero radius). Moreover, in these cases, a complete set of boundary conditions follows directly from (A1a)–(A1d) under the assumption of finiteness of all state variables of the problem at the points where the constitutive parameters change abruptly.

Using (A1a)–(A1d), it is straightforward to prove that the following relations hold for a pair of arbitrary solutions $\mathbf{E}_{1,2}, \mathbf{H}_{1,2}$, $\varphi_{w,1,2}, I_{1,2}$ of these equations with the sources $\mathbf{J}_{1,2}^{\rm ext}, V_{1,2}^{\rm ext}$

$$\nabla \cdot [\mathbf{E}_1 \times \mathbf{H}_2 - \mathbf{E}_2 \times \mathbf{H}_1] = \mathbf{E}_2 \cdot \mathbf{J}_1^{\rm ext} - \mathbf{E}_1 \cdot \mathbf{J}_2^{\rm ext} + \frac{E_{z,2} I_1 - E_{z,1} I_2}{a^2} \quad \text{(A2a)}$$

$$\frac{\partial}{\partial z}(\varphi_{w,1} I_2 - \varphi_{w,2} I_1) = E_{z,1} I_2 - E_{z,2} I_1 + V_1^{\rm ext} I_2 - V_2^{\rm ext} I_1 \quad \text{(A2b)}$$

Combining (A2a) and (A2b), we obtain the Lorentz lemma valid for the general case of the uniaxial wire medium with position-dependent constitutive parameters

$$\nabla \cdot \left[\mathbf{E}_1 \times \mathbf{H}_2 - \mathbf{E}_2 \times \mathbf{H}_1 + \frac{\varphi_{w,1} I_2 - \varphi_{w,2} I_1}{a^2} \hat{\mathbf{z}} \right] = \mathbf{E}_2 \cdot \mathbf{J}_1^{\rm ext} - \mathbf{E}_1 \cdot \mathbf{J}_2^{\rm ext} + \frac{V_1^{\rm ext} I_2 - V_2^{\rm ext} I_1}{a^2}. \quad \text{(A3)}$$

From this lemma, the reciprocity theorem can be formulated by integrating over a volume V with boundary S,

$$\int_S \hat{\mathbf{n}} \cdot \left[\mathbf{E}_1 \times \mathbf{H}_2 - \mathbf{E}_2 \times \mathbf{H}_1 + \frac{\varphi_{w,1} I_2 - \varphi_{w,2} I_1}{a^2} \hat{\mathbf{z}} \right] dS = \int \left[\mathbf{E}_2 \cdot \mathbf{J}_1^{\rm ext} - \mathbf{E}_1 \cdot \mathbf{J}_2^{\rm ext} + \frac{V_1^{\rm ext} I_2 - V_2^{\rm ext} I_1}{a^2} \right] dV \quad \text{(A4)}$$

when V is taken as the whole space the left-hand side surface integral vanishes provided the fields satisfy radiation boundary conditions at infinity, which results in

$$\int_{V_1} \left(\mathbf{E}_2 \cdot \mathbf{J}_1^{\rm ext} + \frac{V_1^{\rm ext} I_2}{a^2} \right) dV = \int_{V_2} \left(\mathbf{E}_1 \cdot \mathbf{J}_2^{\rm ext} + \frac{V_2^{\rm ext} I_1}{a^2} \right) dV \quad \text{(A5)}$$

where the integration volumes $V_{1,2}$ fully enclose the source regions in the two problems.

REFERENCES

[1] D. Sievenpiper, L. Zhang, R. Broas, N. Alexopolous, and E. Yablonovitch, "High-impedance electromagnetic surfaces with a forbidden frequency band," *IEEE Trans. Microw. Theory Techn.*, vol. 47, no. 11, pp. 2059–2074, Nov. 1999.

[2] H. Y. Yang, R. Kim, and D. R. Jackson, "Design consideration for modeless integrated circuit substrates using planar periodic patches," *IEEE Trans. Microw. Theory Techn.*, vol. 48, no. 12, pp. 2233–2239, Dec. 2000.

[3] R. F. J. Broas, D. F. Sievenpiper, and E. Yablonovitch, "A high-impedance ground plane applied to a cellphone handset geometry," *IEEE Trans. Microw. Theory Techn.*, vol. 49, no. 7, pp. 1262–1265, Jul. 2001.

[4] F. Yang and Y. Rahmat-Samii, "Reflection phase characterizations of the EBG ground plane for low profile wire antenna applications," *IEEE Trans. Antennas Propag.*, vol. 51, no. 10, pp. 2691–2703, Oct. 2003.

[5] F. Yang and Y. Rahmat-Samii, "Polarization-dependent electromagnetic bandgap (PDEBG) structures: Designs and applications," *Microw. Opt. Technol. Lett.*, vol. 41, pp. 439–444, Jun. 2004.

[6] F. Yang, A. Aminian, and Y. Rahmat-Samii, "A novel surface wave antenna design using a thin periodically loaded ground plane," *Microw. Opt. Technol. Lett.*, vol. 47, pp. 240–245, Nov. 2005.

[7] H. Mosallaei and K. Sarabandi, "Antenna miniaturization and bandwidth enhancement using a reactive impedance substrate," *IEEE Trans. Antennas Propag.*, vol. 52, no. 9, pp. 2403–2414, Sep. 2004.

[8] A. P. Feresidis, G. Goussetis, S. Wang, and J. C. Vardaxoglou, "Artificial magnetic conductor surfaces and their application to low-profile high-gain planar antennas," *IEEE Trans. Antennas Propag.*, vol. 53, no. 1, pp. 209–215, Jan. 2005.

[9] S. Clavijo, R. E. Díaz, and W. E. McKinzie, III, "Design methodology for Sievenpiper high-impedance surfaces: An artificial magnetic conductor for positive gain electrically small antennas," *IEEE Trans. Antennas Propag.*, vol. 51, no. 10, pp. 2678–2690, Oct. 2003.

[10] S. A. Tretyakov, *Analytical Modeling in Applied Electromagnetics*. Norwood, MA, USA: Artech House, 2003, ch. 6.

[11] M. G. Silveirinha and A. B. Yakovlev, "Negative refraction by a uniaxial wire medium with suppressed spatial dispersion," *Phys. Rev. B, Condens. Matter*, vol. 81, Jun. 2010, Art. ID 233105.

[12] C. S. R. Kaipa, A. B. Yakovlev, S. I. Maslovski, and M. G. Silveirinha, "Indefinite dielectric response and all-angle negative refraction in a structure with deeply-subwavelength inclusions," *Phys. Rev. B, Condens. Matter*, vol. 84, Oct. 2011, Art. ID 165135.

[13] C. S. R. Kaipa and A. B. Yakovlev, "Partial focusing by a bulk metamaterial formed by a periodically loaded wire medium with impedance insertions," *J. Appl. Phys.*, vol. 112, Dec. 2012, Art. ID 124902.

[14] C. S. R. Kaipa, A. B. Yakovlev, S. I. Maslovski, and M. G. Silveirinha, "Near-field imaging with a loaded wire medium," *Phys. Rev. B, Condens. Matter*, vol. 86, p. , Oct. 2012, Art. ID 155103.

[15] O. Luukkonen, M. G. Silveirinha, A. B. Yakovlev, C. R. Simovski, I. S. Nefedov, and S. A. Tretyakov, "Effects of spatial dispersion on reflection from mushroom-type artificial impedance surfaces," *IEEE Trans. Microw. Theory Techn.*, vol. 57, no. 11, pp. 2692–2699, Nov. 2009.

[16] A. B. Yakovlev, M. G. Silveirinha, O. Luukkonen, C. R. Simovski, I. S. Nefedov, and S. A. Tretyakov, "Characterization of surface-wave and leaky-wave propagation on wire-medium slabs and mushroom structures based on local and non-local homogenization models," *IEEE Trans. Microw. Theory Techn.*, vol. 57, no. 10, pp. 2700–2714, Oct. 2009.

[17] C. S. R. Kaipa, A. B. Yakovlev, S. I. Maslovski, and M. G. Silveirinha, "Mushroom-type high-impedance surface with loaded vias: Homogenization model and ultrathin design," *IEEE Antennas Wireless Propag. Lett.*, vol. 10, pp. 1503–1506, Dec. 2011.

[18] P. A. Belov, R. Marques, S. I. Maslovski, I. S. Nefedov, M. Silveirinha, C. R. Simovski, and S. A. Tretyakov, "Strong spatial dispersion in wire media in the very large wavelength limit," *Phys. Rev. B, Condens. Matter*, vol. 67, Mar. 2003, Art. ID 113103.

[19] M. G. Silveirinha, "Nonlocal homogenization model for a periodic array of epsilon–negative rods," *Phys. Rev. E, Stat. Phys. Plasmas Fluids Relat. Interdiscip. Top.*, vol. 73, Apr. 2006, Art. ID 046612.

[20] S. I. Maslovski and M. G. Silveirinha, "Nonlocal permittivity from a quasi-static model for a class of wire media," *Phys. Rev. B, Condens. Matter*, vol. 80, Dec. 2009, Art. ID 245101.

[21] M. G. Silveirinha, "Additional boundary condition for the wire medium," *IEEE Trans. Antennas Propag.*, vol. 54, no. 6, pp. 1766–1780, Jun. 2006.

[22] M. G. Silveirinha, C. A. Fernandes, and J. R. Costa, "Additional boundary condition for a wire medium connected to a metallic surface," *New J. Phys.*, vol. 10, May 2008, Art. ID 053011.

[23] M. G. Silveirinha, "Additional boundary conditions for nonconnected wire media," *New J. Phys.*, vol. 11, Nov. 2009, Art. ID 113016.

[24] S. I. Maslovski, T. A. Morgado, M. G. Silveirinha, C. S. R. Kaipa, and A. B. Yakovlev, "Generalized additional boundary conditions for wire media," *New J. Phys.*, vol. 12, Nov. 2010, Art. ID 113047.

[25] M. G. Silveirinha, "Effective medium response of metallic nanowire arrays with a Kerr-type dielectric host," *Phys. Rev. B, Condens. Matter*, vol. 87, Apr. 2013, Art. ID 165127.

[26] O. Luukkonen, C. Simovski, G. Granet, G. Goussetis, D. Lioubtchenko, A. V. Raisanen, and S. A. Tretyakov, "Simple and accurate analytical model of planar grids and high-impedance surfaces comprising metal strips or patches," *IEEE Trans. Antennas Propag.*, vol. 56, no. 6, pp. 1624–1632, Jun. 2008.
[27] L. Onsager, "Reciprocal relations in irreversible processes," *Phys. Rev.*, vol. 37, pp. 405–426, Feb. 1931.
[28] H. B. G. Casimir, "On Onsager's principle of microscopic reversibility," *Rev. Mod. Phys.*, vol. 17, pp. 343–350, Apr. 1945.
[29] M. G. Silveirinha and S. I. Maslovski, "Radiation from elementary sources in a uniaxial wire medium," *Phys. Rev. B, Condens. Matter*, vol. 85, Apr. 2012, Art. ID 155125.
[30] CST Microwave Studio. CST GmbH, CITY, Germany, 2013. [Online]. Available: http://www.cst.com
[31] C. Mateo-Segura, G. Goussetis, and A. P. Feresidis, "Resonant effects and near-field enhancement in perturbed arrays of metal dipoles," *IEEE Trans. Antennas Propag.*, vol. 58, no. 8, pp. 2523–2530, Aug. 2010.
[32] D. E. Fernandes, S. I. Maslovski, G. W. Hanson, and M. G. Silveirinha, "Fano resonances in nested wire media," *Phys. Rev. B, Condens. Matter*, vol. 88, Apr. 2013, Art. ID 045130.
[33] M. G. Silveirinha, C. A. Fernandes, and J. R. Costa, "Electromagnetic characterization of textured surfaces formed by metallic pins," *IEEE Trans. Antennas Propag.*, vol. 56, no. 2, pp. 405–415, Feb. 2008.

David E. Fernandes was born in Coimbra, Portugal, in 1987. He received the "Mestrado Integrado" degree in electrical and computer engineering from the University of Coimbra, Coimbra, Portugal, in 2010, and is currently working toward the Ph.D. degree in electrical and computer engineering from the University of Coimbra.

His research interests include light propagation and manipulation in electromagnetic and quantum metamaterials.

Stanislav I. Maslovski, photograph and biography not available at time of publication.

Mário G. Silveirinha (S'99–M'03) received the "Licenciado" degree in electrical engineering from the University of Coimbra, Coimbra, Portugal, in 1998, and the Ph.D. degree in electrical and computer engineering from the Instituto Superior Técnico (IST), Technical University of Lisbon, Lisbon, Portugal, in 2003.

He is currently an Associate Professor with the University of Coimbra. His research interests include electromagnetic wave propagation in structured materials and effective medium theory.